Arc reattachment driven by a turbulent boundary layer: Implications for the sweeping of lightning arcs along aircraft

Article *in* Journal of Physics D Applied Physics · August 2016

DOI: 10.1088/0022-3727/49/37/375204

CITATION
1

READS
349

4 authors, including:

J. Peraire
Massachusetts Institute of Technology
330 PUBLICATIONS **14,543** CITATIONS

SEE PROFILE

Manuel Martinez-Sanchez
Massachusetts Institute of Technology
300 PUBLICATIONS **4,656** CITATIONS

SEE PROFILE

IOP Publishing Journal of Physics D: Applied Physics
J. Phys. D: Appl. Phys. **49** (2016) 375204 (14pp) doi:10.1088/0022-3727/49/37/375204

Arc reattachment driven by a turbulent boundary layer: implications for the sweeping of lightning arcs along aircraft

C Guerra-Garcia, N C Nguyen, J Peraire and M Martinez-Sanchez

Department of Aeronautics and Astronautics, Massachusetts Institute of Technology, Cambridge, MA, 02139, USA

E-mail: cguerrag@mit.edu

Received 5 May 2016, revised 21 July 2016
Accepted for publication 28 July 2016
Published 19 August 2016

Abstract

A lightning channel attached to an aircraft in flight will be swept along the aircraft's surface in response to the relative velocity between the arc's root (attached to a moving electrode) and the bulk of the arc, which is stationary with respect to the air. During this process, the reattachment of the arc to new locations often occurs. The detailed description of this *swept stroke* is still at an early stage of research, and it entails the interaction between an electrical arc and the flow boundary layer. In this paper we examine the implications of the structure of the boundary layer for the arc sweeping and reattachment process by considering different velocity profiles, both for laminar and turbulent flow, as well as a high fidelity description, using large eddy simulation, of transitional flow over an airfoil. It is found that the local velocity fluctuations in a turbulent flow may be important contributors to the reattachment of the arc, through a combination of an increased potential drop along the arc and local approaches of the arc to the surface. Specific flow features, such as the presence of a laminar recirculation bubble, can also contribute to the possibility of reattachment.

Keywords: arc reattachment, lightning arc, swept stroke, aircraft lightning protection

(Some figures may appear in colour only in the online journal)

1. Introduction

The problem of a lightning strike to aircraft presents two main differences compared to lightning strike to ground based structures [1, 2]. On the one hand, the aircraft is a floating conductive body in the presence of an ambient electric field. As such, it becomes polarized with one end becoming positively charged and the opposite end becoming negatively charged, even under zero net charge conditions. This effect significantly enhances the electric field on the aircraft's surface and its vicinity, and the amplification can be sufficient to trigger a bidirectional leader from the body [3, 4]. Through this mechanism, that is responsible for over 90% of the lightning strikes to aircraft [5], the aircraft becomes the trigger of the lightning discharge; meaning that lightning would not have occurred in the absence of the aircraft.

On the other hand, once the lightning arc has been established, the arc develops between a stationary electrode (the cloud or the ground) and a moving electrode (the aircraft) [6]. That is, the majority of the arc's length is stationary with respect to the air but the segment close to the surface has a relative velocity as a consequence of the aircraft's motion. The segment in close proximity to the aircraft body is elongated, or *swept*. This can lead to a *reattachment* of the arc to a new attachment point along the aircraft's surface [6, 7].

Insight into the arc's inception physics and the swept stroke phase, can help predict the initial attachment points of the arc to the aircraft, as well as the possible reattachment points due to the sweeping of the arc. Determining where these points are located is crucial in terms of ensuring that adequate protection measures are embedded in the vehicle. The exercise of determining the most vulnerable zones of the aircraft, from the lightning strike perspective, is usually referred to as *zoning* [8].

In this work, we focus on the *sweeping* of a lightning arc for a given initial attachment point. This problem entails the complex interaction between an electrical arc and a fluid

boundary layer. Note that the problem of an arc in crossflow and the reattachment phenomenon is not specific to the aircraft-lightning interaction case, as it closely resembles the phenomena encountered in magnetically-driven arcs [9, 10]; and has important implications in the development of plasma torches [11–19].

In the context of the sweeping of lightning arcs along aircraft, the problem has been previously studied both experimentally, through flight campaigns [7, 20, 21] and laboratory experiments [6, 22, 23]; as well as analyzed theoretically [5, 24–31]. In particular, previous theoretical work has dealt with the sweeping of an arc over a flat plate convected by a parallel laminar flow, as defined by the Blasius boundary layer profile [25, 27, 28, 30, 31]; or otherwise, when considering complex 3D objects such as an aircraft, the inviscid solution of the flow is used (potential flow), while ignoring the effects of the viscous boundary layer [5, 25, 26, 29].

In this work, we expand on the findings from the literature by moving beyond the Blasius solution and exploring the effect of important characteristics, found in real boundary layers of aircraft, on the arc reattachment process. In particular, we consider the evolution of an arc in a turbulent boundary layer profile; the effect of instantaneous and local velocity fluctuations; as well as other flow effects like laminar to turbulent flow transition.

2. Arc reattachment and arc reconnection criteria

2.1. Arc reattachment

A detailed evaluation of the behavior of the lightning arc along an aircraft's surface would require simultaneous solution of the physics of the arc column and the transverse fluid flow. Moreover, the self-consistent modeling of the reattachment process would need the incorporation of very detailed physics, including non-equilibrium plasma effects [19]. In this work, we choose to consider a detailed flow model, since the focus is on the effect of realistic flow effects on the dynamics of the arc, at the expense of using a simpler model for the arc and the reattachment physics.

The arc model considered is that presented in [5, 25, 26, 29]. More specifically, the arc is modeled as a fluid line attached to the surface of the body (the mobile electrode). The elongation of the arc under a prescribed velocity field is then evaluated by integrating the trajectories of the fluid particles belonging to that line, following a Lagrangian approach.

For the flow field model, we will employ different velocity profiles, both for laminar and turbulent flow, as well as a high fidelity description, using large eddy simulation, of transitional flow over an airfoil. Consideration of high Reynolds number turbulent flow, instead of laminar flow, introduces (1) a sharper velocity profile; and (2) the effects of having a time-dependent arc meandering due to the turbulent fluctuations. This second effect, as will be seen, may be a dominant contribution to the re-strike process, as it leads to close approaches of the arc to the wall.

The problem is solved in the frame of reference of the aircraft [31]: the electrode representing the aircraft's surface is immobile whereas the flow outside the boundary layer has a velocity u_e along x. Figure 1 illustrates the evolution of the arc being convected by a 2D boundary layer, from which the reattachment criterion is derived.

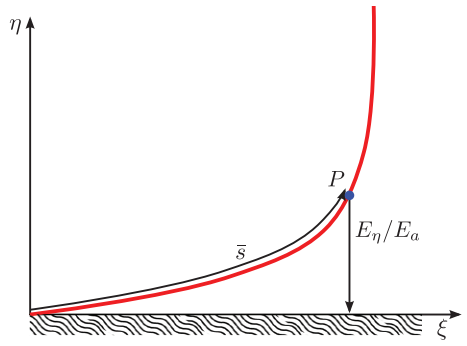

Figure 1. Evaluation of the criterion for arc reattachment based on the gas gap between arc and surface reaching the breakdown threshold. The arc is marked in red. Reference system is that of the electrode.

In particular, for the 2D boundary layer profile pictured in figure 1, the velocity is a function of the coordinate orthogonal to the wall, y, which has been non-dimensionalized by the thickness of the boundary layer δ ($\eta = y/\delta$),

$$\bar{u}(\eta) = \frac{u}{u_e}. \tag{1}$$

The elongation of the arc, as convected by this velocity field becomes

$$\xi = \frac{x}{\delta} = \frac{u_e t}{\delta}\bar{u}(\eta), \tag{2}$$

$$\bar{s} = \frac{s}{\delta} = \int_0^\eta \sqrt{1 + \left(\frac{\mathrm{d}\xi}{\mathrm{d}\eta}\right)^2}\,\mathrm{d}\eta, \tag{3}$$

where ξ is the coordinate along the wall and $\bar{s}$ the normalized arc length at point P given by (ξ, η).

Inside the arc, an electric field of magnitude E_{int} develops. For the case of a stationary free burning arc with current of 1000 A, the authors of [25] quote an internal electric field of 150 V m^{-1}. In the presence of a transverse aerodynamic flow, the internal electric field depends not only on the current but also on the velocity due to the increased thermal losses

$$\frac{E_{\mathrm{int}}}{E_a} = \bar{E}_{\mathrm{int}}(\bar{u}), \tag{4}$$

where E_a is a reference field (dependent on the arc current) and $\bar{E}_{\mathrm{int}}(\bar{u})$ is a normalized internal electric field that depends on the nondimensional velocity $\bar{u}$. Note that for a freely convected arc, such as the one here considered, the field enhancement may not be very important, since the relative velocity between air and arc will be negligible. For the particular case in which the internal electric field of the arc can be considered constant, $\bar{E}_{\mathrm{int}}(\bar{u}) = 1$ and E_a is the internal field of the arc. The authors of [25, 32], consider this dependency of the form $\bar{E}_{\mathrm{int}}(\bar{u}) = \bar{u}^{2/3}$.

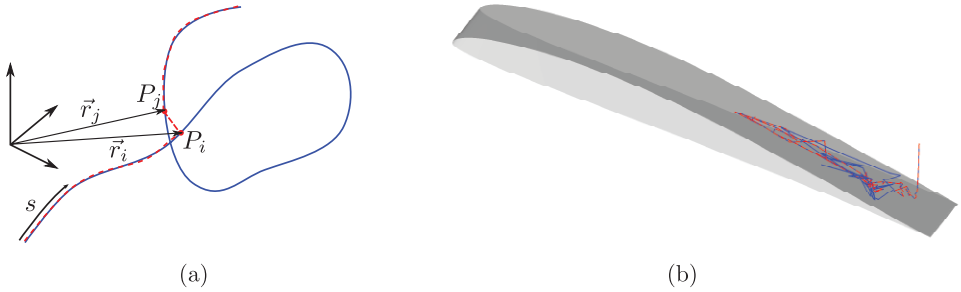

Figure 2. Algorithm and example of arc reconnection for a highly tortuous arc. (a) Reconnection criterion: before (blue line) versus after (red line). (b) Computed reconnection example: arc before (blue line) versus arc after (red line).

Taking the surface as the reference potential $\Phi = 0$, the electrostatic potential for any given point P along the arc can be evaluated by integrating the internal electric field along it

$$\frac{\Phi_p}{E_a\delta} = \int_0^{\bar{s}} \bar{E}_{\text{int}}(\bar{u}(\bar{s}))\mathrm{d}\bar{s}. \tag{5}$$

The potential difference between any point P in the arc and the electrode surface results in an electric field, acting on the gas gap between them, of value

$$\frac{E_\eta}{E_a} = \frac{\Phi_p}{E_a y} = \frac{\Phi_p}{(E_a\delta)\eta} = \frac{\int_0^{\bar{s}} \bar{E}_{\text{int}}(\bar{u}(\bar{s}))\mathrm{d}\bar{s}}{\eta}. \tag{6}$$

In the case of a constant internal field of the arc, this equation reduces to

$$\frac{E_\eta}{E_a} = \frac{\bar{s}}{\eta}. \tag{7}$$

The reattachment criterion is reached whenever the electric field in the air gap, between arc and surface, surpasses the electrical breakdown threshold of the air, E_{bk}, that is, whenever

$$\frac{E_\eta}{E_a} \geqslant \frac{E_{\text{bk}}}{E_a} = \bar{E}_{\text{th}}. \tag{8}$$

The criterion is easily extended to a 3D geometry, as required in section 6.

2.2. Arc reconnection

Previous studies in the literature predict 2D arc geometries that are monotonic, $\frac{\mathrm{d}\eta}{\mathrm{d}\bar{s}} > 0$, as a result of using a laminar boundary layer profile [25, 27, 28, 30, 31], see figure 1. When considering 3D unsteady turbulent boundary layer profiles (such as the ones encountered in real aircraft), the arc can present high tortuosity, becoming entangled in itself and introducing the possibility of *arc reconnection*. Following the same rationale as in section 2.1, arc reconnection is here predicted whenever the electric field between two points in the arc, P_i and P_j, is above the breakdown threshold of the air gap. It will depend, not only on the proximity of the two points, $d_{i,j}$, but also on the length of the segment of arc between them, $|s_j - s_i|$, since this last term will define the potential drop between the two points $|\Phi_j - \Phi_i|$, see figure 2:

$$d_{i,j} = |\vec{r}_i - \vec{r}_j|, \tag{9}$$

$$\bar{E}_{i,j} = \frac{E_{i,j}}{E_a} = \frac{|\Phi_j - \Phi_i|}{E_a d_{i,j}} = \frac{|\int_{\bar{s}_i}^{\bar{s}_j} \bar{E}_{\text{int}}(\bar{u}(\bar{s}))d\bar{s}|}{d_{i,j}/\delta}. \tag{10}$$

It reduces to the following equation

$$\bar{E}_{i,j} = \frac{|s_j - s_i|}{d_{i,j}}, \tag{11}$$

when we assume that the arc has a constant internal electric field.

The arc reconnection criterion is therefore defined:

$$\bar{E}_{i,j} \geqslant \bar{E}_{\text{th}}, \tag{12}$$

where, if reconnection is predicted, a new straight segment of arc is established between the points P_j and P_i, and the old segment of arc (much longer) will fade away, since the current will now flow through the shortest path which will be more energetically favorable. Figure 2(a) illustrates the arc reconnection criterion for a 3D arc, where the arc before reconnection is marked in blue and the new arc, after reconnection, is marked in red. Figure 2(b) shows an actual computation for the 3D unsteady turbulent flow field over an airfoil (section (6)), that predicts reconnection. If reconnection is predicted, the tortuosity and length of the arc suddenly drop. The tracking of the evolution of the arc can be continued by restarting the time integration from the new arc and evaluating the modified potential drop along the arc assuming the internal electric field is $\bar{E}_{\text{int}}$.

The impact of tortuosity on arc elongation (the arc length s will be higher for a tortuous arc as compared to a monotonic arc) has been considered before, as introduced by magnetic effects [33] or an anisotropic conductivity of the arc [34]. Here, we introduce a new source of tortuosity, for which the unsteady turbulent flow is responsible.

Note that the arc reconnection condition, as well as the reattachment criterion in section 2.1, assume an infinitesimally thin arc. In reality, there must be a second reconnection/reattachment condition based on electrical contact between two points, when the minimum distance between two distinct points in the arc, or between arc and wall, is of the order of the arc diameter (as used by [33]). The complication is defining precisely that *diameter*, since it may or may not include a corona halo around the arc. In addition, [31] showed that the criterion for reattachment might need to be

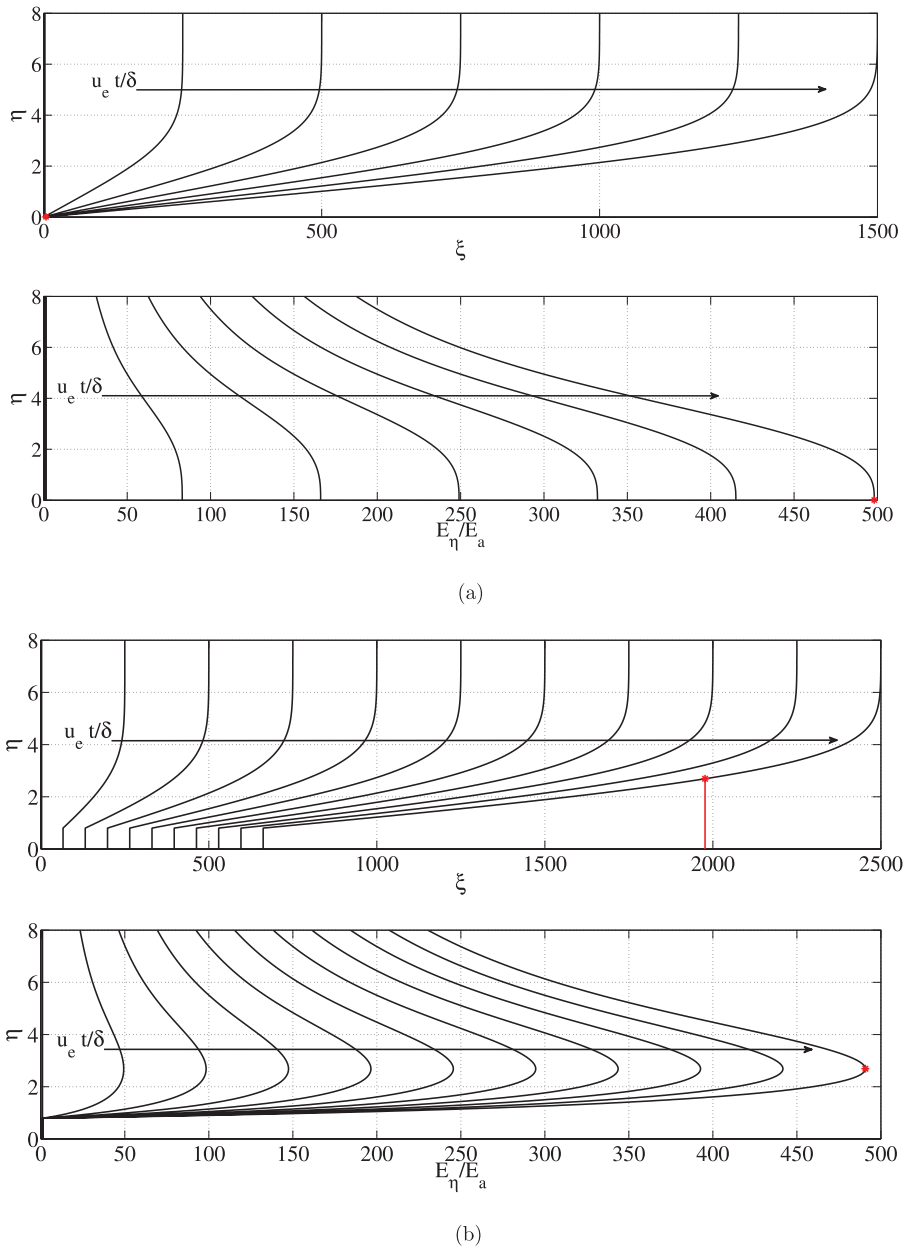

Figure 3. Blasius profile with constant internal arc electric field. The profiles presented are spaced by $u_e\Delta t/\delta = 250$. (a) Blasius profile. (b) Blasius profile with vertical arc segment of length $l_a/\delta = 0.8$ (as in [25]).

revisited for an arc diameter of the order of the boundary layer thickness, since they predicted that the lightning arc would be stuck to the surface with no observable air gap between surface and arc. In what follows, the implications of a finite arc diameter will not be considered, and will be explored in future work.

3. Arc evolution in 2D boundary layer profiles

3.1. Laminar boundary layer flow: the Blasius profile

We begin the discussion by considering the laminar boundary layer over a semi-infinite plate parallel to a uniform 2D flow with velocity u_e. The solution to this problem is the well known Blasius boundary layer profile [35].

Figure 3(a) shows the evolution of an arc, initially at $\xi = 0$ (arc orthogonal to the plate), as a function of time, $u_e t/\delta$, and as convected by the Blasius velocity profile. The evolution of the arc needs to be tracked numerically, since the Blasius profile does not have an analytic solution. The profiles presented are spaced by $u_e\Delta t/\delta = 250$, and δ is taken as a constant (ignoring the actual growth of the boundary layer with the streamwise coordinate ξ). In the case of a constant internal electric field in the arc, $\bar{E}_{\rm int} = 1$, the electric field in the air gap between arc and plate, E_η/E_a, is also shown. The breakdown threshold, $\bar{E}_{\rm th}$, is here taken as 500 (to compare with the data in [25] using $E_{\rm bk} = 1.5 \cdot 10^6$ V m^{-1}, at 0.5 atm, and $E_a = 3$ kV m^{-1}, for $u_e = 50$ m s^{-1} and $I = 600$ A).

In this situation, for a laminar boundary layer and a constant internal arc electric field, there is no likely reattachment

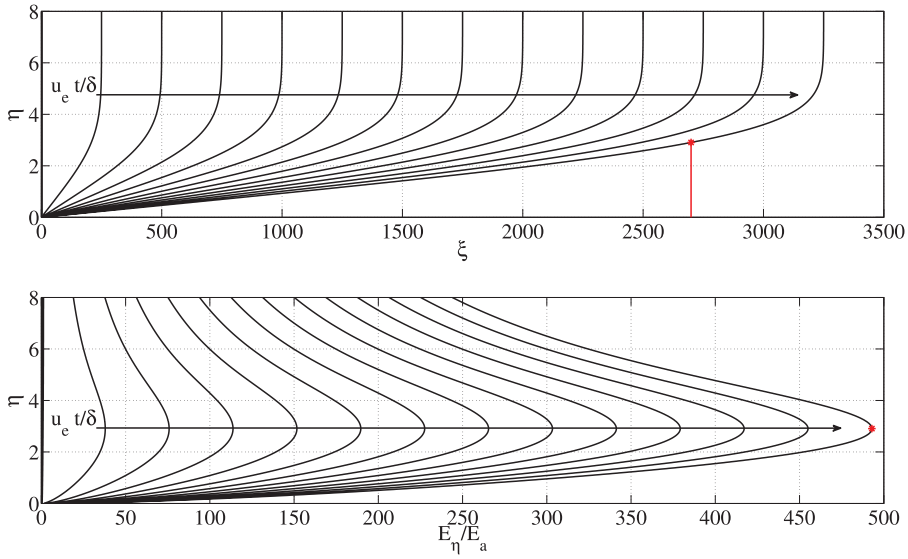

Figure 4. Blasius profile with internal arc electric field dependent on transverse flow velocity, $\bar{E}_{\text{int}}(\bar{u}) = \bar{u}^{2/3}$. The profiles presented are spaced by $u_e \Delta t/\delta = 250$.

point because the maximum of E_η/E_a is always encountered at the root of the arc itself, so the attachment point will remain at the root indefinitely. This suggests that arc elongation by a laminar boundary layer is not sufficient to provide arc reattachment and another effect must be responsible for this process to take place. However, beyond the instantaneous arc elongation shown in figure 3(a) (when the maximum field has reached the breakdown threshold) continuous sweeping of the arc along the electrode surface can occur. This can be explained since, if the same elongation were to continue, more and more of the arc's points would surpass the breakdown threshold of the air gap between arc and plate. Therefore, continuous sweeping is possible, but a skipping or reattaching arc will not occur, based on the flow field structure alone.

The authors of [25] introduce two additional effects: (1) a vertical segment of the arc at the arc root and (2) the dependency of the internal electric field of the arc with the velocity profile.

In the first case, a vertical segment at the attachment point, that is convected at the velocity of the upper most point of that segment, translates into a continuous sweeping of the arc along the surface instead of having a fixed root at $(\xi, \eta) = (0, 0)$, see figure 3(b). Moreover, in terms of the likelihood of reattachment, the inclusion of this vertical segment introduces the possibility of a re-strike. This observation is independent of whether or not the anchor point stays in place, so long as there is a stiff root. At any given time, figure 3(b) shows that the electric field between the arc and the plate, E_η/E_a, is now maximum at a point that is not the original arc root ($\eta = 0$), around $\eta \approx 2.7$. This point becomes a possible reattachment point. More specifically if $E_\eta/E_a \geqslant \bar{E}_{\text{th}}$ reattachment will occur, as marked by the new arc segment in red, and the old segment fades away. The reattachment point occurs at $u_e t/\delta \approx 1980$, which corresponds to an arc dwell time (time the lightning channel attaches to a given point) of ~ 40 ms and a skip distance (distance between two consecutive attachments) of ~ 2 m, comparable to the values reported in [25] (δ is taken as 1 mm).

The second effect, the dependency of the arc's internal field with the flow velocity, is shown in figure 4. Introducing this effect also allows for the existence of a point along the arc of maximum E_η/E_a, that is, a possible reattachment point if the breakdown threshold is reached. Using the same values as in the previous example, the reattachment point happens for $u_e t/\delta \approx 2700$, which corresponds to an arc dwelling time of ~ 54 ms and a skip distance of ~ 2.7 m.

All in all, the arc reattachment driven by a laminar boundary layer can only occur if the internal arc electric field depends on the velocity profile or, otherwise, if there is a stiff arc segment at the root.

For an arc that is convected by the flow, as the one considered in this analysis, the relative velocity of the arc with respect to the air will be close to zero, and therefore cooling of the arc and modification of the internal field due to convective thermal losses cannot be justified.

On the other hand, whereas the rationale behind inserting a vertical arc segment in [25] is not clear, it is well known that strong cathodic, and to some extent anodic, electromagnetically induced jets occur at arc attachments that could be indeed responsible for a stiffening of the arc at its root. In this situation, the anchor point would stay in place, and the vertical segment would be exposed to the transverse and vertical flow contributions, leading to a partial tilting of this segment. A simple estimate of the vertical velocity induced by such a jet gives: $v_j = \sqrt{\mu_0 I^2/(2\pi^2 \rho R_r^2)}$, with μ_0 the magnetic permeability, ρ the density and R_r the arc radius at the root [36]. For example, for $I = 600$ A, $R_r = 1$ mm and $\rho = 0.6$ kg m^{-3}, the velocity of the jet is $v_j \approx 200$ m s^{-1}! The penetration length of a jet into a transverse flow is given by [37] as $l_j = \sqrt{\dot{m}_j v_j/(\rho u_e^2)}$, which corresponds to the square root of the jet-to-cross flow momentum flux ratio. For the case of interest, this length becomes $l_j = \sqrt{\mu_0 I^2/(8\pi\rho u_e^2)}$, and for the values considered $l_j \approx 3.5$ mm which is of the order of the boundary layer thickness at hand.

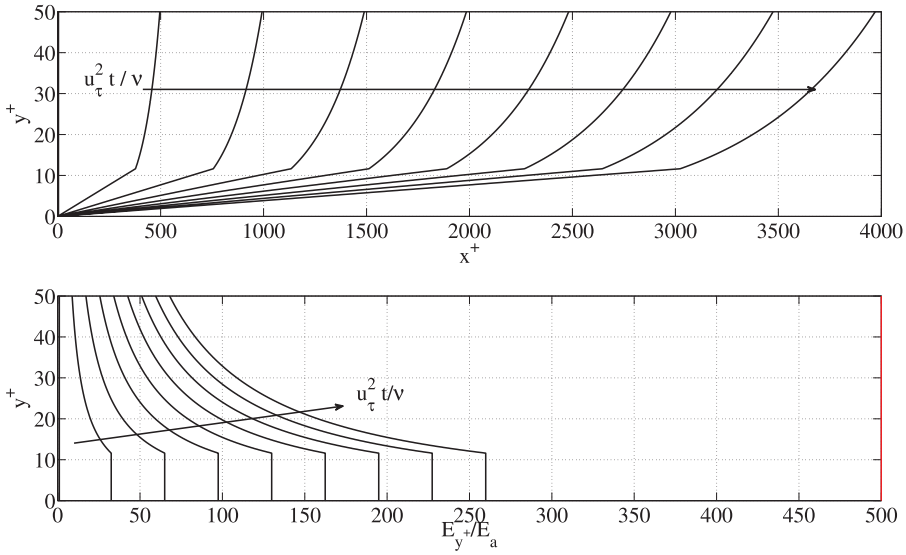

Figure 5. Mean turbulent boundary layer profile (wall layer) with constant internal arc electric field. The profiles presented are spaced by $u_\tau^2 \Delta t/\nu = 32.5$. Note that the sharp corner is smooth in reality but does not affect the behavior.

3.2. Turbulent boundary layer flow: the linear-log wall layer

When considering turbulent flow, as is more representative of the high Reynolds number flow around an aircraft, the boundary layer has a very different appearance. Turbulent flow is characterized by chaotic fluctuations in all three components of the velocity, but for many purposes it is sufficient to evaluate the *mean* velocity field by averaging out the local instantaneous fluctuations. In this averaged sense, a turbulent boundary layer has a three-layer structure: the laminar or linear sublayer, the overlap or log layer (these two layers combined are the so-called wall layer) and the wake or outer layer [35].

The wall layer is generally expressed in terms of wall unit velocity and length scales, that is:

$$u_\tau = \sqrt{\frac{\tau_w}{\rho}}, \qquad l_\tau = \frac{\nu}{u_\tau}, \tag{13}$$

where $\tau_w = \rho u_\tau^2$ is the shear stress at the wall, and ν the kinematic viscosity. The wall velocity is related to the external flow velocity by the friction coefficient $C_f = 2u_\tau^2/u_e^2$. The corresponding nondimensionalized velocity, normal coordinate to the wall, and streamwise coordinate are:

$$u^+ = \frac{u}{u_\tau}, \qquad y^+ = \frac{y}{l_\tau} = \frac{y u_\tau}{\nu}, \qquad x^+ = \frac{x u_\tau}{\nu} = \frac{u_\tau^2 t}{\nu} u^+, \tag{14}$$

which are referred to as the *wall variables*, and play the role of the $\bar{u}$, η, ξ variables introduced in the scaling of the laminar boundary layer analysis. The laminar sublayer is given by:

$$u^+(y^+) = y^+, \tag{15}$$

and the log-layer by:

$$u^+(y^+) = \frac{1}{\kappa} \ln y^+ + B, \tag{16}$$

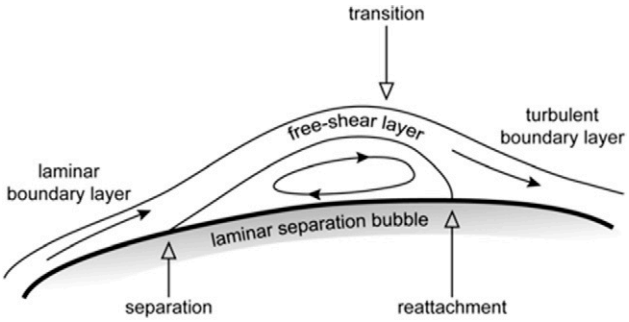

Figure 6. Flow structure in a laminar separation bubble. Reattachment here refers to the *flow* reattachment.

where κ is the von Karman constant, $\kappa = 0.4$, and $B = 5.5$. The minimum of the two pieces is the so-called law of the wall function [35].

The elongation of an arc subjected to this velocity profile is shown in figure 5. The arc is, as before, initially at $x^+ = 0$ (vertical line) and its deformation is shown for different instants of time with $u_\tau^2 \Delta t/\nu = 32.5$, this time step is selected so that a direct comparison can be made to the numerical analysis of figure 11.

Figure 5 shows that the maximum of the electric field developing between the arc and the wall is always located at the initial root of the arc, so there is no possible reattachment point. This leads to the important observation that reattachment driven by the mean turbulent velocity profile, as for the laminar case, is not possible without additional assumptions like a stiff root or a velocity-dependent internal field. Note that, even though a skipping or reattaching arc can not occur (based on the flow effect alone) a continuous sweeping of the arc along the electrode surface is still possible, when the electric field at the arc root reaches the breakdown threshold.

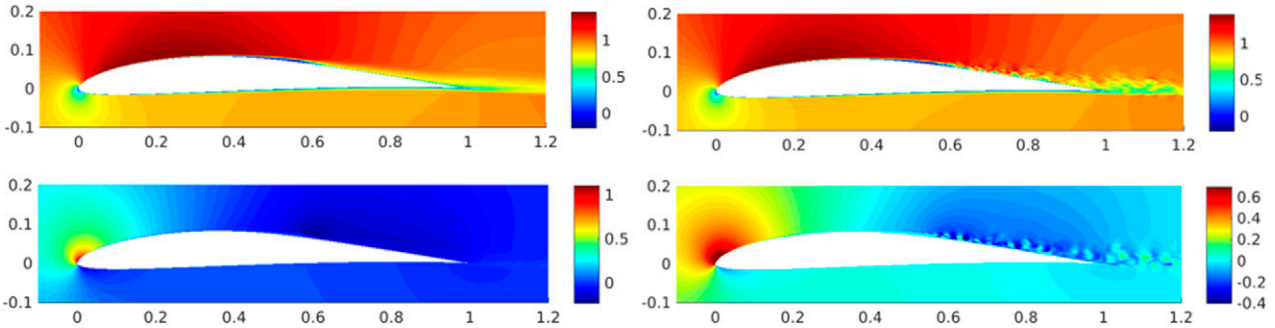

Figure 7. Mean versus instantaneous velocity fields: horizontal instantaneous velocity (top right), horizontal mean velocity (top left), vertical instantaneous velocity (bottom right), and vertical mean velocity (bottom left). x and y coordinates are normalized by the chord, c, and the velocity fields are normalized by the external velocity, u_e.

3.3. Other analytical boundary layer profiles

As an academic exercise, the analysis has been extended to other velocity profiles, such as a power law $\bar{u} = \eta^{1/n}$ $(n = 6)$, or a flat plate with suction, $\bar{u} = 1 - \exp(-v_s y/\nu)$, with v_s the suction velocity. In both these cases, the value of E_η/E_a is maximum at all times at the initial attachment point and a possible reattachment point only appears by artificially including a vertical arc segment at the root.

4. Real effects in high Reynolds number flow: transition and local fluctuations

Flow behavior is governed by the Reynolds number, $\mathrm{Re} = u^* l^*/\nu$, where u^* and l^* are the characteristic velocity and length respectively, and for flow over an airfoil are usually taken as u_e and the chord c. Beyond a certain critical Reynolds number, the flow transitions from laminar to turbulent; with important structure and behavioral modifications. In terms of aerodynamic characteristics, turbulent flows typically present larger wall friction coefficients associated to increased momentum transfer and dissipation; and are more robust to separation of the flow. These same traits will also affect the dynamics of an arc subjected to such a velocity field, as is explored in the following sections. We focus on two effects: (1) transition, and (2) instantaneous local velocity fluctuations.

4.1. Transitional turbulent flow

Transition from laminar to turbulent flow, over airfoils and wings at sufficiently low Reynolds, often takes place in conjuction with a laminar separation bubble: since laminar flows tend to separate more readily than turbulent flows under adverse pressure gradient conditions, see figure 6. The presence of such a flow feature will impact the trajectory of a swept arc.

4.2. Mean and instantaneous velocity fields

In section 3.2, a turbulent boundary layer profile was represented by an analytical expression for the mean velocity field. The real flow field will have, superimposed to this steady mean flow, an unsteady fluctuating part. These fluctuating velocities are 3D and chaotic and with root-square-mean values of $\sim$5% of the external velocity, u_e.

It is here proposed that, instantaneous, local fluctuations of the flow can affect the trajectory of the arc during the sweeping phase and, therefore, it is of interest to evaluate the arc dynamics when considering the time-evolution of the velocity field, and not only its mean value. Figure 7 shows the mean and instantaneous velocity fields for a transitional turbulent flow past an Eppler airfoil at Reynolds number of 300 000, illustrating the laminar bubble separation and turbulent reattachment of the flow. Details about the numerical simulation and the results obtained will be given in the next section.

5. Numerical methods

The main difficulty to numerically simulate transitional turbulent flows is the very small magnitude of the perturbations that get exponentially amplified along the unstable portion of the laminar boundary layer. These small perturbations are ultimately responsible for the so-called non-linear breakdown and transition to turbulence. The amplitude of these instabilities at the location in which the boundary layer becomes unstable is usually many orders of magnitude below the freestream velocity. Therefore, a small amount of numerical dissipation and dispersion is needed to capture them and accurately predict the transition location. Overdissipation may kill these small perturbations and lead to inaccurate prediction. As a result, high-order accurate methods are more favorable than low-order methods to capture the complex dynamics of turbulent flows undergoing transition.

For the large eddy simulation of transitional turbulent flows considered herein, we use the hybridizable discontinuous Galerkin (HDG) method [38–40] to discretize the compressible Navier–Stokes equations. Instead of using a subgrid-scale model to filter the small unresolved scales in the large eddy simulation, we rely on numerical dissipation of the HDG method to deal with these scales. This approach is known as implicit large eddy simulation (ILES) [41–43], which has recently gained considerable attention from researchers in the computational fluid dynamics community because of its easy implementation and robustness.

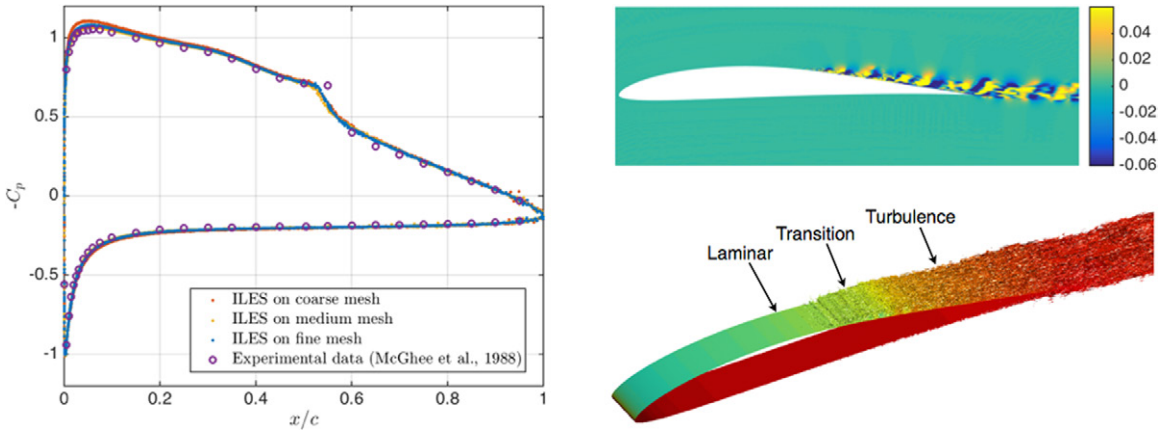

Figure 8. ILES prediction of the transitional flow over the Eppler 387 wing at Reynolds number 300 000, Mach number 0.08, and 4° angle of attack. Pressure coefficient (left), instantaneous spanwise velocity (top right), and iso-surface of the Q-criterion colored by the pressure (bottom right).

Table 1. Details of the computational meshes considered for the Eppler 387 wing.

Mesh	Polynomial degree	No. Elements	Global unknowns	Time step
Coarse	4	64 800	1 959 600 × 5	7.937×10^{-3}
Medium	4	126 360	3 814 380 × 5	6.300×10^{-3}
Fine	4	254 976	7 687 680 × 5	5.000×10^{-3}

Note: Global unknowns indicates the number of coupled unknowns and the ×5 factor accounts for the five components in the Navier–Stokes equations.

The HDG method has many advantages that make it well-suited to ILES of transitional turbulent flows. Like other discontinuous Galerkin (DG) methods, the HDG method is based on a strong mathematical foundation that can be exploited for error estimation and mesh adaptation purposes. It provides local conservation, a stable discretization of the convective operator, and is well-suited for turbulent simulations due to the *ab initio* separation of scales in the variational formulation. Most importantly, the HDG method allows for high-order implementations on complex geometries and unstructured meshes, while being more computationally efficient than other DG methods and even finite volume methods [44].

For a while, ILES of transitional turbulent flows using DG methods was limited to Reynolds numbers of 100 000 or less [45–49]. Recently, ILES of transitional turbulent flows at Reynolds number of 250 000 were performed using the HDG method [44]. Here we will demonstrate this ILES approach on transitional flow past an airfoil and study its effects on the evolution of the arc in terms of reattachment and reconnection. We refer the reader to [44] for the detailed description of our ILES approach using the HDG method. In this spirit, we consider transitional flows over an Eppler 387 wing at Reynolds number of 300 000, Mach number of 0.08, angle of attack of 4.0 degrees, and zero freestream turbulence intensity. The airfoil is extruded in the spanwise direction by a length $0.1c$ and the computational domain extends about 10 chords away from the wing. We choose to perform this simulation because the experimental data reported in [50] are very accurate and reliable to validate our simulation results.

We use polynomials of degree 4 for the spatial approximation and the third-order implicit Runge–Kutta scheme [51] for temporal discretization, leading to a numerical scheme that is fifth-order in space and third-order in time. The computational domain is partitioned using iso-parametric tetrahedral elements. Three meshes and dimensionless time-steps are considered; which correspond to uniform refinement in space and time. The details of these meshes are summarized in table 1.

The simulation results are shown in figure 8. We see that the profiles of the time-averaged pressure coefficient agree very well with the experimental data reported in [50]. Furthermore, we observe grid convergence in the sense that the simulation results converge to the experimental data as the mesh is refined. We observe from the pressure coefficient profiles in figure 8 and the velocity fields in figure 7 that the flow separates on the upper side at $x_{s,f}/c = 0.46$ due to the adverse pressure gradient. This produces a laminar separation bubble and strongly destabilizes the boundary layer; which eventually transitions to turbulence. After transition, the turbulent mixing leads to rapid reattachment at $x_{r,f}/c = 0.55$ and the separation bubble ends. The turbulent boundary layer remains attached all the way until the trailing edge thanks to the resistance to separation provided by the turbulent mixing. Note that the error in the prediction of transition location compared to the experimental value is below $0.005c$ on the coarse mesh. In the next section, we will study the evolution of the arc in this flow field under a wide range of conditions.

6. Arc evolution in transitional 3D turbulent flow over an airfoil

The selected flow field allows us to study the evolution of the arc under a wide range of conditions: mean and time-dependent laminar, transitional, and turbulent flows; as well as evaluate the impact of the initial attachment point relative to the flow structure. In all cases, the internal electric field of the arc is taken as constant.

For comparison with the results in section 3.2, the mean friction coefficient is $C_f = 0.0048$ and the conversion from wall variables to airfoil variables is as follows:

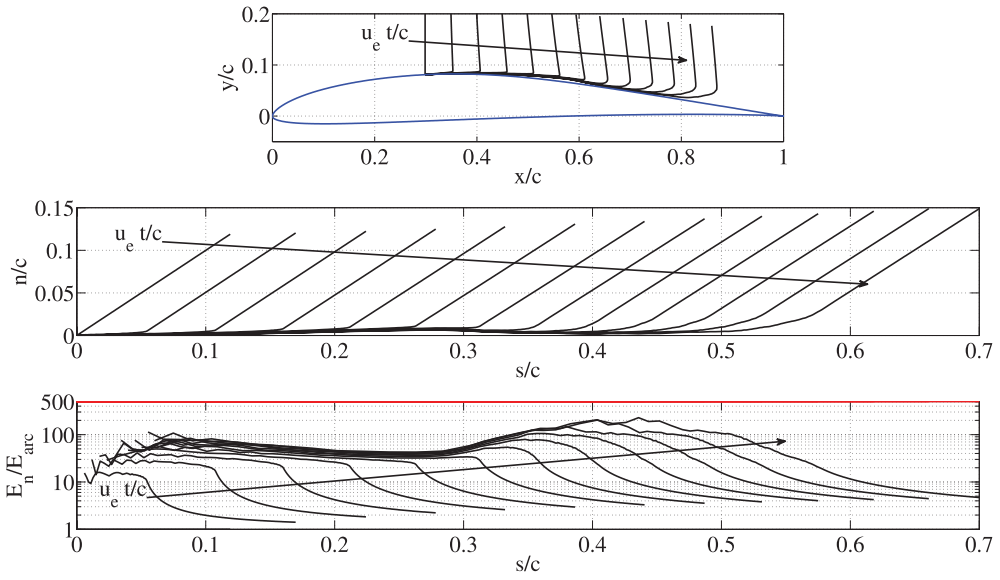

Figure 9. Arc convected by mean velocity profile, initial attachment point in laminar region preceding separation bubble, at $(x/c)_0 = 0.3$. The profiles presented are spaced by $u_e \Delta t/c = 0.04$.

$$\frac{l}{c} = \frac{l u_\tau}{\nu} \frac{1}{\mathrm{Re}} \sqrt{\frac{2}{C_f}}, \qquad \text{for} \quad l = x, y, z, s, \tag{17}$$

$$\frac{u_e t}{c} = \frac{u_\tau^2 t}{\nu} \frac{2}{C_f} \frac{1}{\mathrm{Re}}. \tag{18}$$

These non-dimensional quantities are useful for our analysis in this section.

6.1. Mean velocity field

In this section, the evolution of the arc initially attached to different positions along the chord of the airfoil is evaluated, as convected by the mean velocity field. Table 2 shows the prediction of arc reattachment and reconnection as a function of different initial arc attachment points (in the laminar, transition and turbulent regions). The breakdown threshold is taken as $\bar{E}_{\mathrm{th}} = 500$, as in section 3. Note that the x coordinate is measured from the leading edge of the airfoil, whereas the s coordinate measures the actual arc length and so is measured from its root.

When considering the mean velocity fields, no reconnection nor arc reattachment is predicted, except for a possible reattachment when the arc initially strikes in the recirculation bubble close to the flow reattachment point $(x/c)_0 = 0.6$. Reconnection is not expected since the mean velocity field is essentially 2D, as is the trajectory of the arc. Therefore, the arc does not become entangled or twisted.

The absence of a reattachment point is due to different effects, that depend on the location of the initial attachment point, $(x/c)_0$.

For an arc initially attached in the laminar flow region preceding the separation bubble, e.g. $(x/c)_0 = 0.3$, the arc evolution and electric field between arc and airfoil is shown in figure 9. After the separation bubble, the arc becomes dangerously close to the airfoil surface, as illustrated by the normal coordinate to the surface n/c. In this region, there exists a maximum electric field between arc and surface (maximum of E_n/E_{arc}) that could become a possible reattachment point if the electric field is amplified above the breakdown threshold. For the length of the airfoil considered, this maximum never exceeds the threshold value and reattachment will not occur.

Table 2. Prediction of arc reattachment when using the mean velocity field.

$(x/c)_0$	Is there reattachment?	$(u_e t/c)_r$	$(x/c)_r$	$(s/c)_r$	Is there reconnection?
0.3	No				No
0.4	No				No
0.5	No				No
0.6	Yes	0.24	0.66	0.14	No
0.7	No				No
0.8	No				No

Note: Subscript 0 refers to the initial arc attachment point, r to the arc reattachment condition. x is measured from the leading edge of the airfoil, and s is the elongation of the arc measured from its root. Flow reattachment after the laminar separation bubble occurs at $x_{r,f}/c \approx 0.6$.

In the second case considered, the arc is initially attached in the separation bubble region, close to the flow reattachment location. The arc evolution and electric field between arc and airfoil are shown in figure 10, for the case $(x/c)_0 = 0.6$. Since the arc is initially attached at the end of the laminar separation bubble, it is subjected to a mean turbulent velocity profile which resembles that considered in section 3.2. Similar to the case of the analytical turbulent boundary layer profile in figure 5, the electric field decays along the arc and the maximum field is encountered at the initial arc root. Therefore, there is no likely reattachment point and the attachment point will continue to be the initial one indefinitely. For the numerical evaluation, there is a reattachment point predicted (marked by the red dot in figure 10), this is interpreted as a numerical artifact since it is just a single point raising above the breakdown threshold

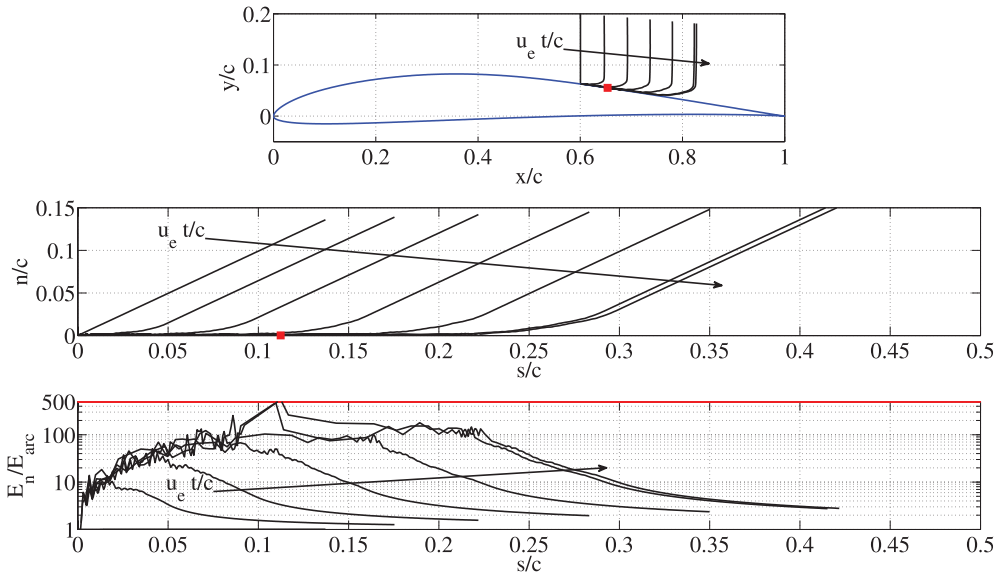

Figure 10. Arc convected by mean velocity profile, initial attachment point in laminar separation bubble, at $(x/c)_0 = 0.6$. The profiles presented are spaced by $u_e\Delta t/c = 0.04$. Reattachment is marked in red.

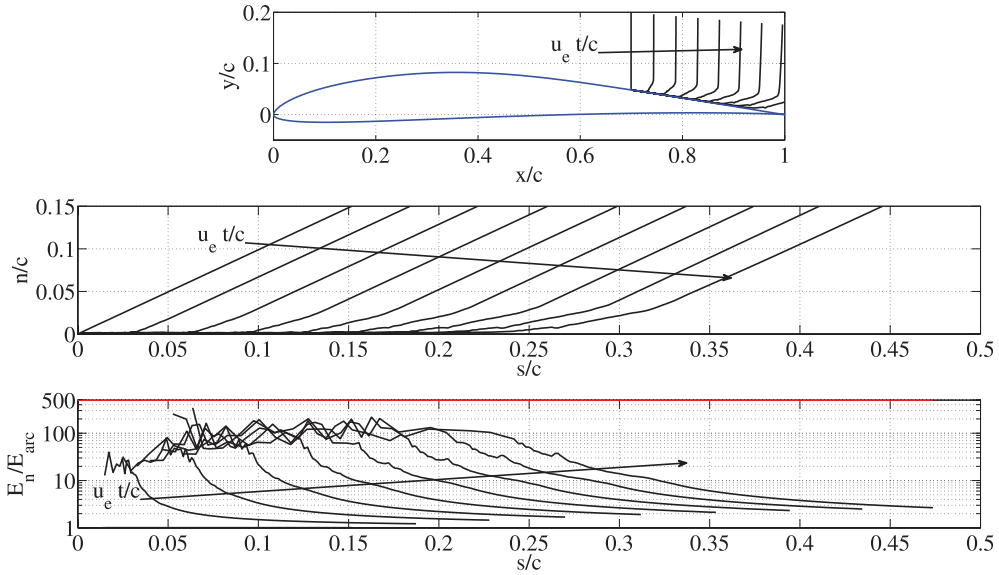

Figure 11. Arc convected by mean velocity profile, initial attachment point in turbulent region after separation bubble, at $(x/c)_0 = 0.7$. The profiles presented are spaced by $u_e\Delta t/c = 0.04$.

and if this value is just slightly higher, then no reattachment would occur.

Finally, for an arc that is initially attached in the turbulent region after the separation bubble, the results are shown in figure 11, for the case $(x/c)_0 = 0.7$. As for the prediction using the analytical turbulent boundary layer profile in section 3.2, the electric field decays along the arc and there is no possible reattachment point since the most favorable attachment location is always the initial arc root.

6.2. Instantaneous velocity field

In reality, the arc trajectory will be driven by the time-dependent evolution of the flow field. The instantaneous fluctuations will complicate the structure and dynamics of the arc

Table 3. Prediction of arc reattachment when using the instantaneous velocity field.

$(x/c)_0$	Is there reattachment?	$(u_e t/c)_r$	$(x/c)_r$	$(s/c)_r$	Is there reconnection?
0.3	Yes	0.29	0.64	0.41	No
0.4	Yes	0.22	0.62	0.27	No
0.5	Yes	0.14	0.61	0.18	No
0.6	Yes	0.08	0.64	0.19	No
0.7	No				No
0.8	No				No

Note: Subscript 0 refers to the initial arc attachment point, r to the reattachment condition. x is measured from the leading edge of the airfoil, and s is the elongation of the arc measured from its root. Flow reattachment after the laminar separation bubble occurs at $x_{r,f}/c \approx 0.6$.

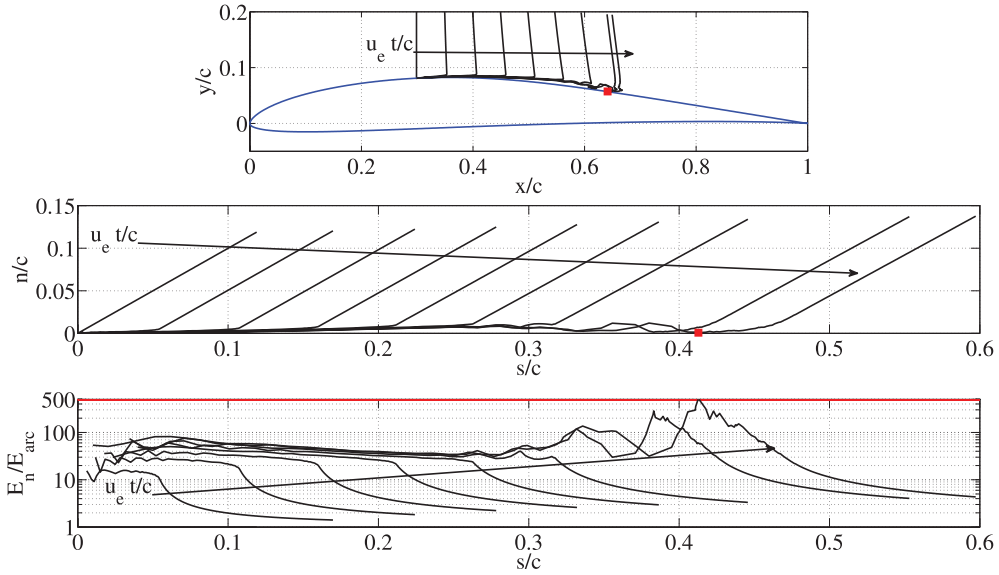

Figure 12. Arc convected by **instantaneous velocity profile**, initial attachment point in laminar region preceding separation bubble, at $(x/c)_0 = 0.3$. The profiles presented are spaced by $u_e\Delta t/c = 0.04$. Reattachment is marked in red.

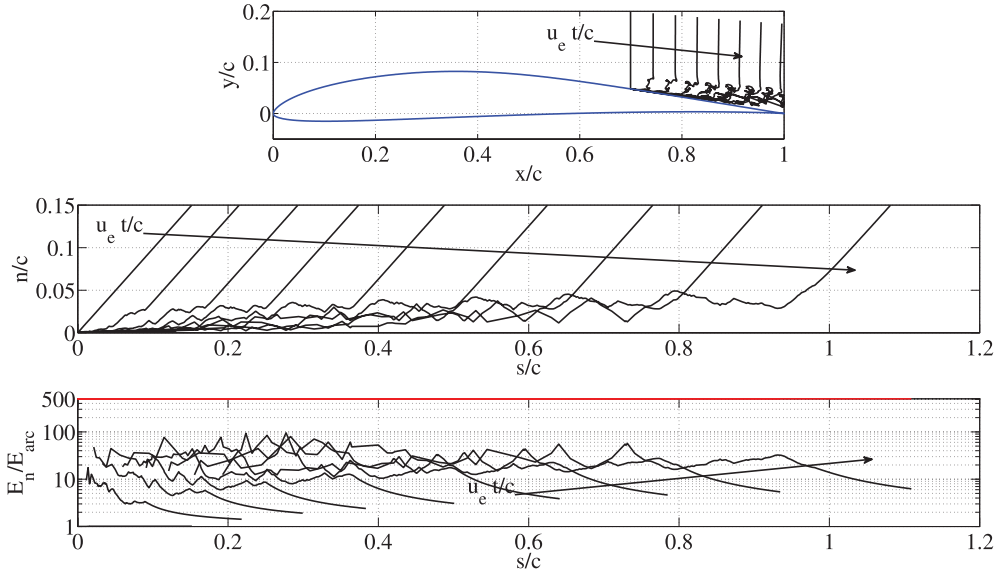

Figure 13. Arc convected by instantaneous velocity profile, initial attachment point in turbulent region after separation bubble, at $(x/c)_0 = 0.7$. The profiles presented are spaced by $u_e\Delta t/c = 0.04$.

leading to a 3D trajectory that can present entanglement and close approaches of the arc with itself. To track the implications of such phenomena, the dynamics of the arc initially attached to different positions along the chord of the airfoil are here evaluated, as convected by the time-evolving velocity field. Table 3 shows the prediction of arc reattachment and reconnection as a function of the initial arc attachment point. For the results presented, calculation of the arc evolution is stopped whenever arc reattachment is predicted or when the arc reaches the trailing edge of the airfoil.

The first observation to be made is that, despite the highly entangled appearance of the arc (as seen in figure 13), arc reconnection is not observed in any of the cases considered since arc reattachment occurred before any reconnection could take place. However, if the trajectory of the arc was integrated over longer times, reconnection could indeed happen, as shown in figure 2(b).

The absence of reconnection can be explained by looking at equation (10): even though there might be points along the arc that come to close proximity, the potential drop along the arc is also usually small, being proportional to the arc length between those two points and the relatively low internal electric field of the arc. This can lead to a highly tortuous arc that will not reconnect with itself.

The second observation is that reattachment of the arc is now predicted for those cases in which the initial attachment point occurs before the end of the laminar recirculation bubble. In all cases, the arc reattachment point occurs at $(x/c)_r \approx 0.63$,

which corresponds to the approximate location of the boundary layer reattachment. As an illustrative example, figure 12 shows the arc evolution in the case of $(x/c)_0 = 0.3$ as convected by the instantaneous velocity field. The reattachment point is marked in red, when the electric threshold field, $\bar{E}_{\text{th}}$, is reached. When comparing the solutions for the mean (figure 9) and instantaneous (figure 12) velocity fields, in both cases, the arc becomes very close to the surface after the separation bubble resulting in the existence of a maximum E_n/E_{arc} at that location. In the case of the mean velocity field, this maximum E_n/E_{arc} never reaches the breakdown threshold, due to the limited length of the airfoil chord. On the other hand, reattachment occurs for the instantaneous velocity field because the local velocity fluctuations force a much closer encounter of the arc with the surface. Note that, even though the reattachment condition in figure 12 appears only marginal, if the arc is convected beyond that condition, maximum non-dimensional fields of ~4000 are calculated, so even for higher thresholds (or incorporating an error band in the threshold), turbulence can bring us into that band.

When the initial arc root occurs in the turbulent flow region, $(x/c)_0 > 0.6$, no reattachment is observed despite the high tortuosity that increases the electrical potential drop along the arc (figure 13). The appearance of the electric field between arc and surface is similar to the corresponding case using the mean velocity field, figure 11, in that the general trend of E_n/E_{arc} is to decay along the arc. However, instantaneous fluctuations are now observed and this leads to the existence of a maximum E_n/E_{arc} that could become a possible reattachment point. Nevertheless, due to the short length over which turbulent flow is encountered over the airfoil in this particular case, the threshold is never reached and there is no reattachment. This is a consequence of the transition happening at $x/c \sim 0.6$: if the turbulent boundary layer started developing earlier arc reattachment driven by the instantaneous flow fluctuations would indeed be possible. In actual cases, reattachment is mainly observed when the initial arc attachment is near the nose of an aircraft and a long distance is available for the arc to be stretched along the fuselage. Our simulation is limited by the relatively short chord of the wing considered.

A final comment refers to the predicted tortuosity of the arc driven by the turbulence of the flow. Tortuosity is here defined by comparing the arc length when considering the time-dependent evolution of the arc, to the arc length when considering the mean velocity field: $T = \Delta s_{\text{inst}}/\Delta s_{\text{mean}}$. High tortuosity of the arc leads to longer arc lengths and a corresponding increase of the electric potential drop along the arc. As an example, for an initial attachment of $(x/c)_0 = 0.7$ and for $u_e t/c \approx 0.32$ (last profiles in figures 11 and 13), the length of an arc segment which is initially $(\Delta s/c)_0 = 0.15$, becomes $\Delta s/c = 0.47$ when considering the mean velocity field, and $\Delta s/c = 1.11$ when considering the instantaneous velocity field. These values lead to a tortuosity of $T = 2.4$. The contribution of turbulent fluctuations to tortuosity is important as it increases the potential drop along the arc, and therefore favors breakdown. Note that the magnitude of the tortuosity predicted here is comparable to that induced by the magnetic instability effects, which have already been studied by other authors [33].

7. Conclusions

The reattachment of a long arc along the surface of an aircraft in flight is a complex phenomenon that involves flow and plasma effects. In this manuscript, we explore the implications of the fluid boundary layer structure in this process by performing a large eddy simulation of a transitional flow over an airfoil at Re = 300 k, at the expense of using simple arc and reattachment models. The findings of these studies highlight the importance of a correct description of the flow in order to be able to predict reattachment of the arc. The main conclusions are summarized in what follows:

(a.) The classical boundary layer structure for a semi-infinite flat plate, both for laminar (Blasius profile) and turbulent (linear-log layer) flow, does not allow for arc reattachment. This is a consequence of the electric field, between arc and surface, decreasing along the arc. Note that, even though a skipping or reattaching arc can not occur, a continuous sweeping of the arc along the electrode surface is still possible, when the electric field at the arc root reaches the breakdown threshold.

(b.) When using these simple 2D boundary layer profiles, arc reattachment is only possible if a vertical arc segment is artificially included at the root or by introducing the dependency of the arc internal electric field with the velocity profile. By introducing either of these effects, the electric field between arc and surface presents a maximum that is at a different location than the initial arc root.

(c.) Flow features, such as the presence of a laminar recirculation bubble, can introduce a possible arc reattachment location, through the physical approach of the arc to the surface, as guided by the flow.

(d.) For the evolution of the arc in a turbulent boundary layer over an airfoil, arc reattachment again is not possible when considering the mean velocity field since there is no likely reattachment point.

(e.) By considering the instantaneous local velocity fluctuations, reattachment may become possible due to a local enhancement of the electric field at random locations.

(f.) Incorporation of the instantaneous fluctuations contributes to the favoring of breakdown through two main effects: (1) local approach of the arc to the surface; (2) increased arc length and hence electrical potential drop along the arc.

(g.) The computed magnitude of the tortuosity of the arc due to local turbulent fluctuations is comparable to previously reported values due to magnetic effects. For the case considered, a tortuosity ($T = \Delta s_{\text{inst}}/\Delta s_{\text{mean}}$) greater than 2 was predicted, with the twisting and bending of the arc being solely due to the contribution of turbulence.

(h.) Despite the high arc entanglement encountered in some of the simulations performed, arc reconnection was not predicted as a result of the small electric potential drop along the arc.

The present study accounts for the influence of the flow field alone, a predictive evaluation would need to consider additional effects such as transient electrical current surges or

the effect of surface conditions such as rivets [23] that introduce local electric field enhancements. Future efforts will be devoted to incorporating more detailed models for the arc and reattachment criterion. In addition, the boundary layer considered is not representative of all conditions along a real fuselage in flight, where the Reynolds numbers can be 10–100 times higher. Separation bubbles may not happen then, but the turbulent intensity may be higher, the flows can be fully turbulent, and the available length for arc sweeping will be longer. Future studies will address those conditions, but the lower Reynolds regimes studied in this work (300 k) are valuable and important specially when the lightning arc attaches close to the leading edge of an airfoil or the nose, since the flows there have characteristics of lower Re.

Acknowledgments

This work was supported by The Boeing Company through the strategic universities for Boeing Research and Technology Program. N C Nguyen and J Peraire acknowledge partial support from the Air Force Office of Scientific Research (AFOSR) through Grant No. FA9550-16-1-0214. The authors would like to thank Pablo Fernandez (MIT) for helping with the large eddy simulation and Mark Drela (MIT) for use of his Blasius boundary layer profile solver.

References

[1] Vonnegut B 1965 Electrical Behavior of an Airplane in a Thunderstorm Technical Report No. FAA-ADS-36 to Federal Aviation Agency under contract to Arthur D. Little, Inc.
[2] Uman M A and Rakov V A 2003 *Prog. Aerosp. Sci.* **39** 61–81
[3] Mazur V 1989 *J. Geophys. Res.* **94** 3311–25
[4] Cooray V 2015 *An Introduction to Lightning* (New York: Springer) (doi: 10.1007/978-94-017-8938-7)
[5] Larsson A 2002 *C. R. Phys.* **3** 1423–44
[6] Plumer J A 2012 Laboratory test results and natural lightning strike effects: how well do they compare *Proc. Int. Conf. Lightning Protection* (*Vienna, Austria, 2–7 September*) (doi: 10.1109/ICLP.2012.6344201)
[7] Zaepfel K P, Fisher B D and Ott M S 1985 Direct-strike lightning photographs, swept-flash attachment patterns, and flight conditions for storm hazards '82 *NASA Technical Memorandum* No. 86347 (NASA Langley Research Center, Hampton, Virginia)
[8] Lalande P and Delannoy A 2012 Numerical Methods for Zoning Computation *Aerosp. Lab* AL05 1–15
[9] Novak J P and Fuchs V 1974 *Proc. IEE* **121** 81–4
[10] Meyer T N 1977 *IEEE Trans. Power Appar. Syst.* **96** 1324–8
[11] Wutzke S A, Pfender E and Eckert E R G 1967 *AIAA J.* **5** 707–14
[12] Wutzke S A, Pfender E and Eckert E R G 1968 *AIAA J.* **6** 1474–82
[13] Duan Z and Heberlein J 2002 *J. Therm. Spray Technol.* **11** 44–51
[14] Li H, Heberlein J and Pfender E 2005 *IEEE Trans. Plasma Sci.* **33** 402–3
[15] Yang G, Cronin P, Heberlein J V and Pfender E 2006 *J. Phys. D: Appl. Phys.* **39** 2764–74
[16] Yang G and Heberlein J V 2007 *J. Phys. D: Appl. Phys.* **40** 5649–62
[17] Yang G and Heberlein J 2007 *Plasma Sources Sci. Technol.* **16** 765–73
[18] Lebouvier A, Delalondre C, Fresnet F, Cauneau F and Fulcheri L 2012 *J. Phys. D: Appl. Phys.* **45** 025204
[19] Trelles J and Modirkhazeni S M 2014 *Comput. Methods Appl. Mech. Eng.* **282** 87–131
[20] Fisher B D 1984 Lightning swept-stroke attachment patterns and flight conditions for storm hazards '81 *NASA Technical Memorandum* No. 86279 (NASA Langley Research Center, Hampton, Virginia)
[21] Laroche P, Blanchet P, Delannoy A and Issac F 2012 Experimental Studies of Lightning Strikes to Aircraft *Aerosp. Lab* AL05 1–5
[22] Clifford D W and McCrary L E 1974 Final report: simulated lightning test Shuttle .03 scale model Report No. MDC A3155, McDonnell Aircraft Company, Saint Louis, Missouri
[23] Dobbing J A and Hanson A W 1978 *IEEE Int. Symp. on Electromagnetic Compatibility* pp 390–5
[24] Larsson A, Lalande P, Bondiou-Clergerie A and Delannoy A 2000 *J. Phys. D: Appl. Phys.* **33** 1866–75
[25] Larsson A, Lalande P and Bondiou-Clergerie A 2000 *J. Phys. D: Appl. Phys.* **33** 1876–83
[26] Larsson A, Bondiou-Clergerie A, Lalande P, Delannoy A and Dupraz S 2001 SAE Technical Paper 2001–01–2876
[27] Lago F, Freton P and Gonzalez J 2005 *IEEE Trans. Plasma Sci.* **33** 434–5
[28] Lago F, Gonzalez J, Freton P, Uhlig F and Lucius N 2006 *J. Phys. D: Appl. Phys.* **39** 2294–310
[29] Broc A, Lalande P, Montreuil E, Moreau J, Delannoy A, Larsson A and Laroche P 2006 *Aerosp. Sci. Technol.* **10** 700–8
[30] Chemartin L, Lalande P, Peyrou B, Chazottes A, Elias P, Delalondre C, Cheron B and Lago F 2012 Direct effects of lightning on aircraft structure: analysis of the thermal, electrical and mechanical constraints *Aerosp. Lab* AL05–09 1–15
[31] Tholin L, Chemartin P and Lalande F 2013 Numerical investigation of the surface effects on the dwell time during the sweeping of lightning arcs *Int. Conf. on Lightning and Static Electricity* (*Seattle, WA, 17–20 September*)
[32] Larsson A, Delannoy A and Lalande P 2005 *Atmos. Res.* **76** 377–85
[33] Chemartin L, Lalande P, Montreuil E, Delalondre C, Cheron B and Lago F 2009 *Atmos. Res.* **91** 371–80
[34] Zohdi T I 2010 *Int. J. Numer. Methods Eng.* **84** 27–46
[35] Drela M 2014 *Flight Vehicle Aerodynamics* (Cambridge, MA: MIT Press)
[36] Pfender E 1983 Plasma Generation *MRS Proc.* **30** 13–35
[37] Broadwell J E and Breidenthal R E 1984 *J. Fluid Mech.* **148** 405–12
[38] Nguyen N C, Peraire J and Cockburn B 2009 *J. Comput. Phys.* **228** 8841–55
[39] Nguyen N C, Peraire J and Cockburn B 2011 *J. Comput. Phys.* **230** 1147–70
[40] Nguyen N C and Peraire J 2012 *J. Comput. Phys.* **231** 5955–88
[41] Boris J P 1990 Chapter: On large eddy simulation using subgrid turbulence models *Whither Turbulence? Turbulence at the Crossroads: Proc. of a Workshop Held at Cornell University (Ithaca, NY, 22–24 March 1989) (*Berlin: Springer) 344–53
[42] Galbraith M and Visbal M 2008 Implicit large eddy simulation of low Reynolds number flow past the SD7003 airfoil *46th AIAA Aerospace sciences meeting and exhibit* (Reno, Nevada, 7–10 January) No. AIAA 2008-225
[43] Visbal M R, Gordnier R E and Galbraith M C 2009 *Exp. Fluids* **46** 903–22

[44] Fernandez P, Nguyen N C, Roca X and Peraire J 2016 Implicit large-Eddy simulation of compressible flows using the interior embedded discontinuous Galerkin method *54th AIAA Aerospace Sciences Meeting* (San Diego, California, 4–8 January) No. AIAA 2016-1332

[45] Uranga A, Persson P O, Drela M and Peraire J 2011 *Int. J. Numer. Methods Eng.* **87** 232–61

[46] Frere A, Hillewaert K, Chivaee H S, Mikkelsen R F and Chatelain P 2015 Cross-validation of numerical and experimental studies of transitional airfoil performance *33rd Wind Energy Symposium* (Kissimmee, Florida, 5–9 January) No. AIAA 2015-0499

[47] Renac F, Llave Plata M, Martin E, Chapelier J B and Couaillier V 2015 *Aghora: a High-Order DG Solver for Turbulent Flow Simulations* In IDIHOM: *A Top-Down Approach, Notes on Numerical Fluid Mechanics and Multidisciplinary Design 128* (Switzerland: Springer) pp 315–35

[48] Wiart C C and Hillewaert K 2015 Development and Validation of a Massively Parallel High-Order Solver for DNS and LES of Industrial Flows In *IDIHOM: A Top-Down Approach, Notes on Numerical Fluid Mechanics and Multidisciplinary Design 128* (Switzerland: Springer) pp 251–92

[49] Murman S M, Diosady L, Garai A and Ceze M 2016 A space-time discontinuous-Galerkin approach for separated flows *54th AIAA Aerospace Sciences Meeting* (San Diego, California, 4–8 January) No. AIAA 2016-1059

[50] McGhee R, Walker B and Millard B 1988 Experimental results for the Eppler 387 airfoil at low Reynolds number in the langley low-turbulence pressure tunnel NASA Technical Memorandum No. 4062 NASA Langley Research Center Langley VA

[51] Alexander R 1977 *SIAM J. Numer. Anal.* **14** 1006–21